PROCEEDINGS OF SPIE

SPIEDigitalLibrary.org/conference-proceedings-of-spie

94 GHz Doppler radar for experimental validation of small UAV micro-Doppler

Matthew Moore, Duncan Robertson, Samiur Rahman

Matthew Moore, Duncan A. Robertson, Samiur Rahman, "94 GHz Doppler radar for experimental validation of small UAV micro-Doppler," Proc. SPIE 12108, Radar Sensor Technology XXVI, 121080S (27 May 2022); doi: 10.1117/12.2618496

SPIE.

Event: SPIE Defense + Commercial Sensing, 2022, Orlando, Florida, United States

94 GHz Doppler radar for experimental validation of small UAV micro-Doppler

Matthew Moore*[a], Duncan A. Robertson[a], Samiur Rahman[a]
[a]SUPA School of Physics & Astronomy, University of St Andrews, St Andrews, Fife KY16 9SS, Scotland

ABSTRACT

The micro-Doppler signature of a small unmanned aerial vehicle (UAV), resulting from the rotation of propeller blades, can be used to differentiate UAVs from other common confusing elements such as birds. Moreover, the micro-Doppler signature varies depending on the shape of individual UAV components such that these signatures can be used to differentiate between different UAV models. In order to investigate how different UAV components affect the signature, a high-fidelity micro-Doppler simulation has been developed previously, capable of generating micro-Doppler returns from 3D CAD models. This simulation requires experimental validation and so a 94 GHz radar has been designed and built for lab-based micro-Doppler measurements of UAV components in CW or FMCW Doppler modes. This allows for controlled experimental recreations of simulated scenarios in which the experimental micro-Doppler signatures of different UAV components can be measured and used for robust simulation validation. In this paper, the radar design will be explained in detail and the radar performance will be reviewed. Chirps are generated around 1 GHz using an Analog Devices AD9914 DDS board and upconverted onto a low phase noise STALO at 6.833 GHz. The upper sideband is filtered and frequency multiplied by 12 to 94 GHz. In FMCW mode the maximum chirp bandwidth is 3 GHz. The receiver is homodyne using a 94 GHz I-Q mixer to de-chirp to baseband. Feedhorn antennas are used for close range lab measurements, but larger antennas could be fitted for longer range outdoor data collection.
Keywords: Micro-Doppler, radar simulation, radar design, simulation validation, unmanned aerial vehicle.

1. INTRODUCTION

In recent years, there has been increased attention on detecting Unmanned Aerial Vehicles (UAVs) because of their potentially malicious implications[1–3]. Micro-Doppler information from a small UAVs, which results from the rotation of the propellers, can be used to differentiate UAVs from common confusing elements such as birds[4]. Furthermore, the micro-Doppler signature varies depending on the shape of the individual UAV propellers such that these signatures can be used to differentiate between different UAV models[5]. In order to take advantage of the micro-Doppler differences for UAV classification, a robust characterization of the micro-Doppler signatures of different UAVs is required. Moreover, it is a challenge to collect sufficient data to train a classifier. Experimental data can be of high quality but is expensive and labor-intensive while simulated data is easier and cheaper but is normally not as realistic. Consequently, a high-fidelity micro-Doppler simulation has been developed previously, capable of generating micro-Doppler returns from 3D CAD models[6]. The point-cloud-based simulation assumes a frequency of 94 GHz due to the detailed micro-Doppler signatures produced at millimeter-wave frequencies[7]. This simulation needs to be experimentally validated using a physical radar operating at the same frequency. Outdoor validations of this simulation are time-consuming and difficult, requiring approval to fly and are limited by availabilities and battery lives of UAVs. Validating indoors is easier and allows for rigorously controlled experimental recreations of simulated scenarios where the experimental micro-Doppler signatures of different UAV components can be used for robust simulation validation. Indoor measurements however require a well calibrated lab-based radar. Thus, a 94 GHz radar has been designed and built for lab-based micro-Doppler measurements of UAV propellers. The simulation uses CW mode while FMCW mode allows for range gating of the return to reduce clutter. This radar will provide a hardware platform for future experiments, including outdoor data collection. For these reasons, the radar operates in both CW and FMCW Doppler modes. Both modes have previously been used for UAV classification.

*mm512@st-andrews.ac.uk; https://mmwave.wp.st-andrews.ac.uk/

Radar Sensor Technology XXVI, edited by Kenneth I. Ranney, Ann M. Raynal, Proc. of SPIE
Vol. 12108, 121080S · © 2022 SPIE · 0277-786X · doi: 10.1117/12.2618496

The unambiguous velocity when using CW radar is limited only by the sampling frequency of the radar, which can be very high such that Doppler information is fully sampled. CW radar has been used for UAV detection[5,8,9] and the high sampling rate has been used to generate micro-Doppler spectrograms representing the propeller's motion. FMCW radar offers range as well as velocity information and can therefore be used to track targets. However, the unambiguous velocity of FMCW radar tends to be limited by the chirp repetition frequency (CRF) of the radar, which means that micro-Doppler information from the fast-moving propellers is aliased and spread across the Doppler spectrum. Nonetheless, the Doppler sidebands from the propeller motion are distinctive when compared with common confusing elements[10,11]. Consequently, FMCW radar can be used for UAV classification[12–15]. A complete study of micro-Doppler information from UAVs needs to consider both CW and FMCW modes.

This validation radar needs to be well-calibrated, operate in both CW and FMCW modes, have the ability to measure targets at very short ranges (of order one meter), have a high Doppler sensitivity, and operate mono-statically and bi-statically as may be required for future measurements. When operating in the FMCW mode, the entire UAV or propeller needs to be contained within a single range bin in order to generate spectrograms showing propeller micro-Doppler. A range resolution requirement of 60 cm is used to ensure this condition is met requiring a chirp bandwidth of 250 MHz. The unambiguous Doppler requirement is dependent on the maximum Doppler returns expected from the UAV, which corresponds to the propeller blade-tip Doppler. The maximum blade-tip Doppler is given by Equation 1.

$$max\ tip\ Doppler = \frac{4\pi \times propeller\ radial\ length\ \times rotation\ rate\ \times radar\ freq}{c} \qquad 1$$

UAV propeller's rotation rates depend on the model of UAV, however, rotation rates around 100 Hz have been measured experimentally for UAVs in flight[4]. Most of the unambiguous Doppler indoor measurements will be done in CW mode. However, for the indoor lab-based setup, the FMCW radar should be able to fully sample the propeller rotation when the motor is idling at 10 Hz, anticipated for a DJI Phantom 3 Standard propeller setup. The DJI Phantom 3 Standard uses a propeller with a 12.5 cm radius such that, for a 10 Hz rotation rate, the maximum Doppler return is 4.9 kHz. This would require a minimum chirp repetition frequency (CRF) of 9.8 kHz, as specified by Nyquist sampling theorem, although exceeding this to allow for some over-sampling is advantageous. To this end, a candidate CRF of 10.8 kHz is selected here, which can be derived from an integer division of the 10 MHz reference. This CRF results in an unambiguous velocity of ±8.6 m/s. For a coherent processing interval of 128 chirps the Doppler resolution would be 84.4 Hz. A sampling rate of 714 kHz has been suggested, which is derived from a separate integer division of the 10 MHz reference and is an integer multiple of the CRF. This gives a maximum instrumented intermediate frequency (IF) of 357 kHz and a maximum instrumented range of 19.2 m, which is more than sufficient for indoor measurements. The proposed radar parameters for the FMCW mode are shown in Table 1.

FMCW	
Parameter	***Value***
Bandwidth	250 MHz
Range resolution	60 cm
CRF	10.8 kHz
Chirp length	89.6 µs
Unambiguous velocity	$\pm$ 8.6 m/s
Sampling rate	714 kHz
Max instrumented IF frequency	357 kHz
Max instrumented range	19.2 m
Doppler resolution	84.4 Hz

Table 1: Proposed radar parameters for FMCW mode.

2. SYSTEM DESIGN

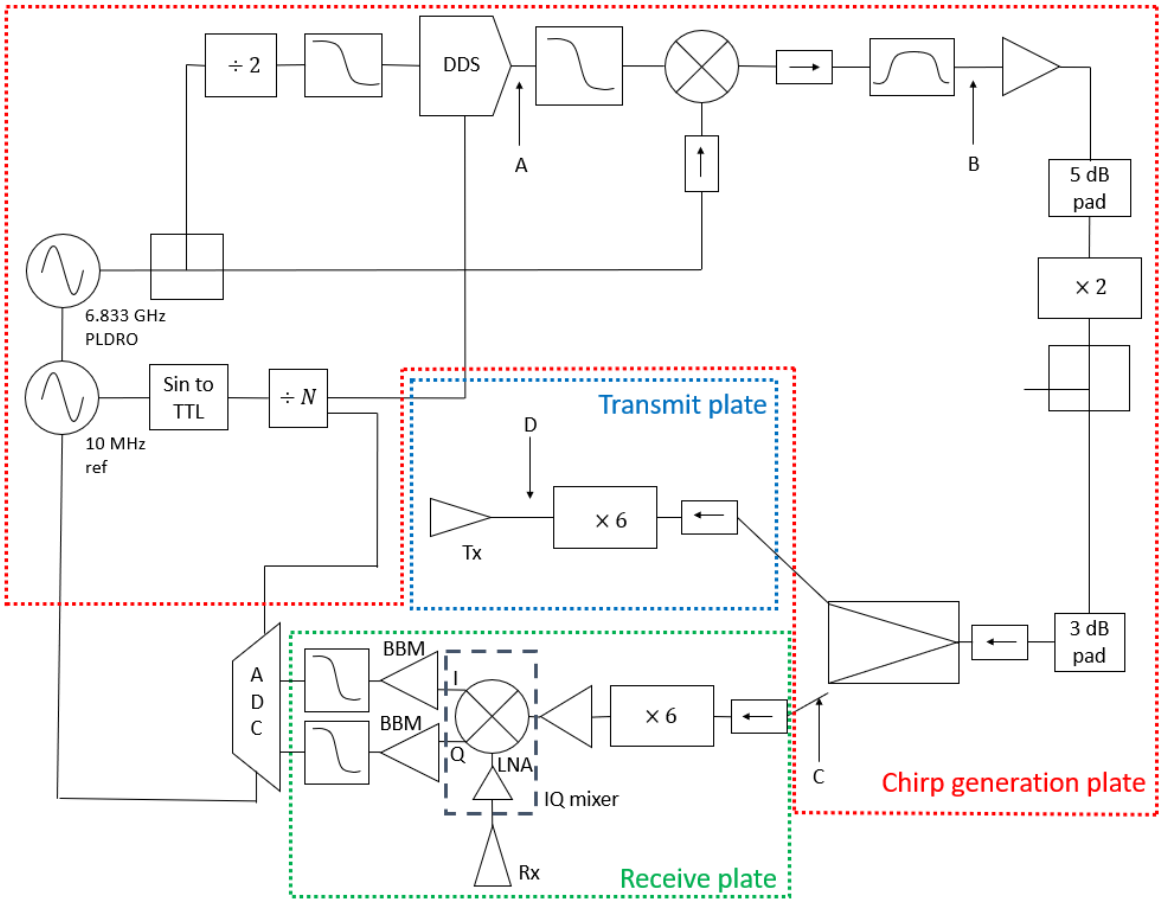

Figure 1: Block diagram showing radar design, plate locations of components and points where chirp spectra are presented later.

The radar design is shown in Figure 1 where the plate locations of the radar components have also been marked, as will be discussed in Section 4. The radar is a dual-antenna homodyne system capable of operating in both CW and FMCW modes. Chirps (FMCW mode) or a single tone (CW mode) are generated by the Analog Devices AD9914 direct digital synthesizer (DDS) clocked at 3.4 GHz and upconverted onto a local oscillator (LO) at 6.833 GHz. The resulting upper sideband at 7.8 GHz is selected using a bandpass filter. A 20 dB gain amplifier and 5 dB pad are used to amplify the signal by 15 dB to satisfy the input requirement for the frequency doubler. The resulting 15.6 GHz signal is passed through a -20 dB directional coupler to provide a monitor point. A 3dB power divider splits the signal to drive the transmit and receive x6 multipliers, resulting in two copies of the signal at 94 GHz. On the transmit side, the output of the x6 multiplier is passed directly into the transmit antenna. On the receive side, an IQ mixer with integral low noise amplifier on the RF port has been selected to enable unambiguous Doppler measurements in CW mode. The 94 GHz signal copy is used as the local oscillator signal to pump the IQ mixer and mix with the received signal from the receive antenna. The I and Q IF outputs of the mixer are amplified using a baseband module (BBM), and then filtered by an anti-alias filter, before being sampled by an analog-to-digital converter (ADC). Since the transmit and receive channels use separate chains, they could be fed via long cables and separated in space, enabling bistatic measurements. For short range lab measurements, feedhorn antennas will be used but larger antennas could be fitted for longer range outdoor measurements.

A 6.833 GHz phase locked dielectric resonator oscillator (PLDRO) provides the first mixer's LO signal and the DDS clock (after passing through an HMC432 divide by two board). This device has been used because of its very low phase noise, which is desirable in a UAV detection radar, where small targets are to be detected in the presence of very bright targets (such as trees)[15]. All other frequencies used in this radar (chirp trigger and the ADC sample and trigger frequencies) are derived from a 10 MHz reference. This 10 MHz reference is also used as the reference signal for the PLDRO. This means that the radar is fully coherent, essential for measuring Doppler information.

2.1 Frequency characterization

Every component in the radar was characterized to validate the radar's performance and measure the RF budget. Passive device measurements at lower frequencies were performed by using an HP8510C vector network analyzer. In general, active device measurements were performed by using an Anritsu MG3692C signal generator and Rohde & Schwarz FSP40 spectrum analyzer in computer-controlled frequency step increments. It was found that the spectrum analyzer's power accuracy deteriorated significantly at 15 GHz[16]. As a result, the signal generator and HP437B power meter were used for measurements at 15 GHz (with 8481A power sensor) and at 94 GHz (with W8486A power sensor). Furthermore, the chirp spectra were measured at every point in the chain. A sample of these at monitor points A, B, C and D (shown in Figure 1) are given in Figure 2 - Figure 5 below.

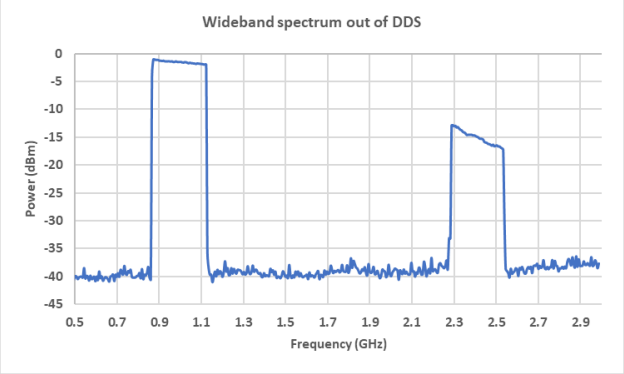

Figure 2: Monitor point A - Wideband spectrum out of DDS around 1 GHz with the image frequency band around 2.4 GHz, prior to filtering.

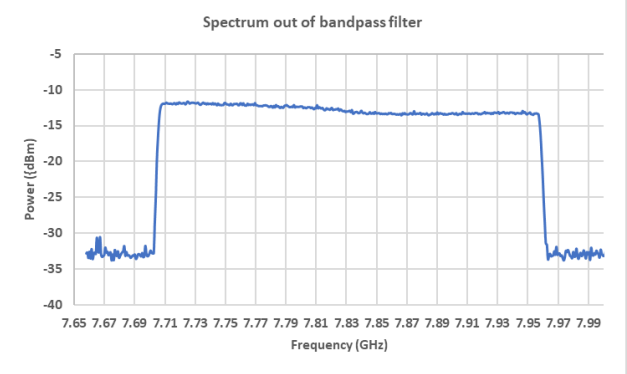

Figure 3: Monitor point B - Chirp spectrum after bandpass filter.

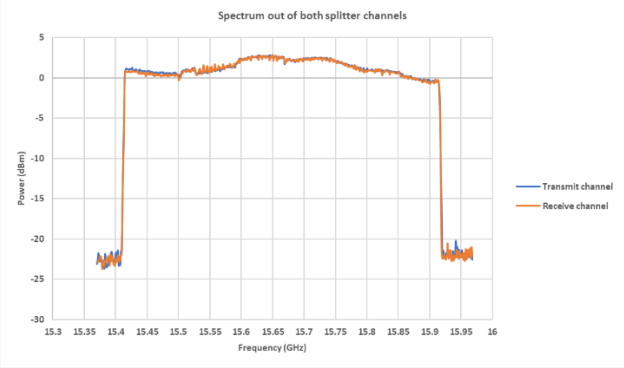

Figure 4: Monitor point C - Chirp spectra out of two splitter channels.

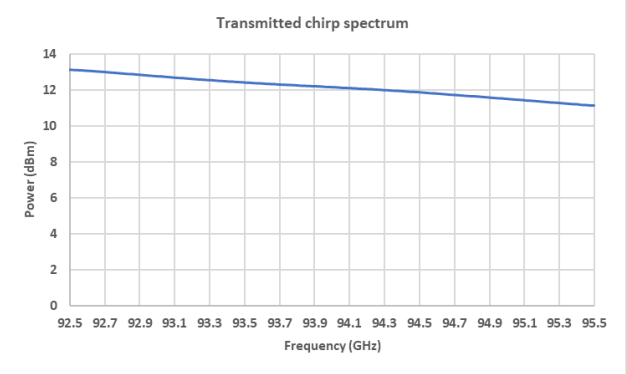

Figure 5: Monitor point D - Transmitted chirp spectrum.

The maximum possible bandwidth is limited by the bandpass filter, which has a passband of 250 MHz. Following the cumulative frequency multiplication by 12, the maximum bandwidth of the radar is 3 GHz, equating to a range resolution of 5 cm. For generating spectrograms of UAV components, the entire UAV needs to be contained within one range bin, so a bandwidth of 250 MHz (at 94 GHz) was chosen giving a range resolution of 60 cm. The ability to reduce the range bin size is advantageous for future applications of this radar, possibly including ISAR imaging.

2.2 IF amplification

The radar is intended to provide micro-Doppler information for UAV components, including propellers. Many of the important, and potentially classifiable, micro-Doppler features exist at low Doppler frequencies (< 10 kHz). These include blade flash – where the propeller blade falls perpendicular to the line of sight of the radar and the coherent summation of the scattering points along the propeller result in a sudden increase in radar return, or a flash [17]. Consequently, appropriate

intermediate frequency (IF) amplification is an important concern for this radar and constant gain down to very low IF frequencies is required. To meet this need, a pre-existing custom-built base-band module (BBM) was used. A simplified design for this module is shown in Figure 6.

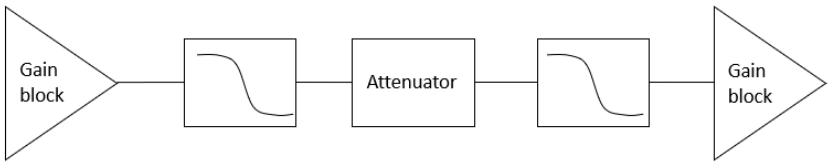

Figure 6: Simplified design for the base-band module.

The noise figure of the BBM is limited by the noise of the front-end device, and as such a low noise Mini-Circuits GALI-52 amplifier has been used for the first gain block with a noise figure of ~3 dB. After this, the two 15 MHz low-pass filters are used as anti-alias filters, where the double filter combination results in a steeper roll-off, although external anti-alias filters are used in this radar to account for the lower sampling rate used. The intermediate attenuator is used to decouple the two devices. Finally, a Mini-Circuits GALI-84 high gain amplifier has been used as the final gain block, to allow for the signal to be sent down long cables after amplification. The low frequency roll-off of this amplifier is shown in Figure 7.

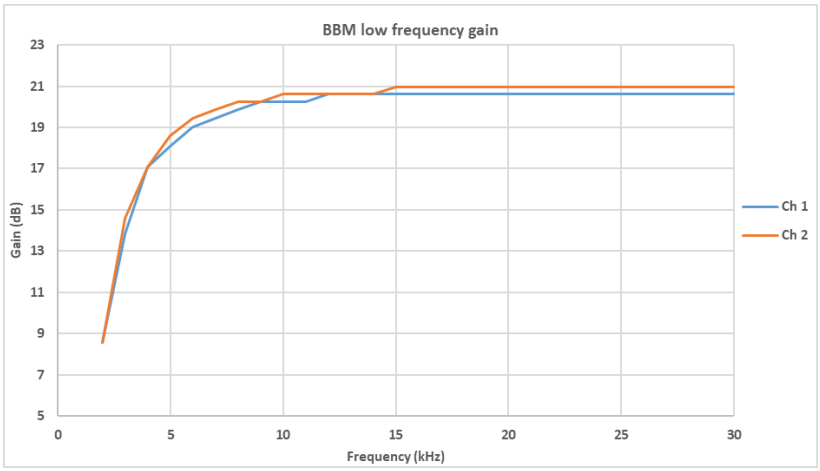

Figure 7: Low frequency response of base-band module.

3. DDS CHIRP OPTIMIZATION

3.1 Spur crossing experiment

A DDS based architecture has been used because it offers very low phase noise chirps, high linearity, and very fast chirps. However, DDSs are known to create spurious signals, or spurs, along with the main signal whose frequencies are deterministic and depend on the position of the main signal and the clock frequency[18]. The relative amplitude of the spurs below the carrier tone varies with frequency and DDS model; in general the average spur level increases with clock frequency. For the AD9914 clocked at 3.4 GHz, the typical spur level is around -50 dBc. During the characterization process, the positions of the AD9914 spurs were measured on the spectrum analyzer as the output frequency was varied from 100 to 1360 MHz (shown in Figure 8). The desired output frequency of the DDS increases linearly, however, some spurious terms can also be seen, emerging at 2 GHz when the output frequency is at 476 Hz and 712 MHz. These dominant spurs then decrease linearly as the output frequency increases such that they cross the output frequency at 856 MHz and 1140 MHz respectively. The 1140 MHz spur crossing has been selected as of particular interest because it corresponds to a three-way crossing – where two separate spurs cross the main signal. The spur crossings are of interest because of their potential interference with the DDS output frequency, either through intermodulation in the mixers or through the additional spectral energy they impart, leading to a broadband increase in the noise level.

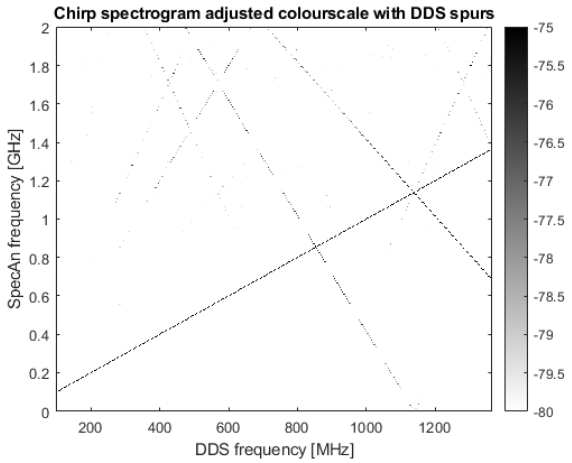

Figure 8: DDS output showing desired output and spurs.

In order to investigate the effects of spur crossings on radar performance, a cable radar was built using the 7.833 GHz signal from the radar circuit combined with a power splitter, a 100 ns delay line, and a 4-10 GHz mixer. A diagram showing the delay line experiment is shown in Figure 9.

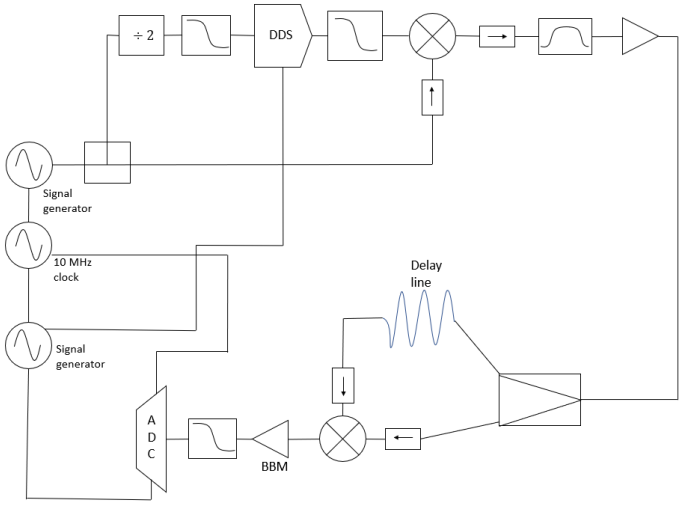

Figure 9: Delay line experiment setup.

The chirp was mixed against a copy of the chirp that had passed through the delay line. The frequency offset resulting from the delay could be measured in the IF signal and was equivalent to a target at 15 m range. This setup enabled testing of how the DDS spurs affect a real radar system, especially around spur crossings. Two separate chirp frequencies were used, where both chirps contained the 1140 MHz triple spur crossing at different points. For a chirp length of 100 μs the spur-signal crossing time could be predicted – see Table 2.

Chirp start frequency (MHz)	1015	950
Chirp stop frequency (MHz)	1265	1200
Predicted spur crossing time (μs)	50	76

Table 2: Chirp frequencies and spur crossing predictions.

The IF mixer output in the time-domain was measured using a Rohde & Schwarz RTO 1004 oscilloscope sampling at 5 GSa/s. Only a very minor disturbance was found at the appropriate times in the IF signal. To increase the clarity of the artifact, the RF (delay-line) signal was disconnected, and the delay-line signal was terminated into a 50-ohm load. Then, the mixer's response to a swept LO containing the spur crossing was measured. The results are shown in Figure 10 and Figure 11. The spur crossing is visible in both cases and appears at the expected time within the signal. The spur crossing artifact has been enlarged for increased clarity in both figures.

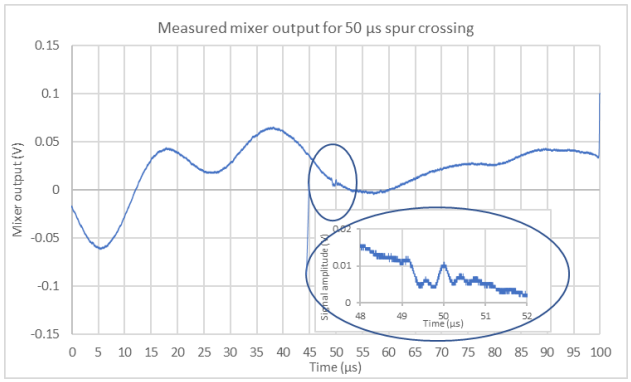

Figure 10: Measured mixer output for spur crossing at 50 µs.

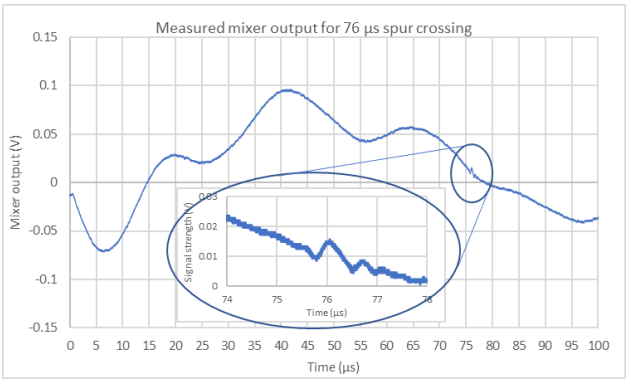

Figure 11: Measured mixer output for spur crossing at 76 µs.

The spectra of the IF signals with and without the spur crossing were compared to test if there would be a broadband increase in the noise level associated with the impulse nature of the spur crossing – see Figure 12. No substantial spectral differences were found between the two signals. The spur crossing does not have sufficient spectral energy to affect the spectrum of the IF signal significantly. To further investigate this effect, a simulation implemented in MATLAB was created that determines the spur crossing artifact power required to affect the noise level. The IF signal was modelled as containing three components: a background white Gaussian noise at -80 dBm, a random walk representing the inherent frequency variation of the mixer, and a single oscillation of a sinusoidal function with varying power levels representing the spur crossing. No significant spectral differences were simulated until the spur-crossing reached a power of -35 dBm, shown in Figure 14, equivalent to -15 dBc below the carrier for the bench radar experiments at 7.833 GHz. In these experiments, the measured spur-crossings are at a sufficient power below the carrier (~ -50 dBc) as to not affect the resulting spectra. It should be noted, though, that the frequency multipliers may cause spectral regrowth of spurs so the relative spur level in W-band may be higher.

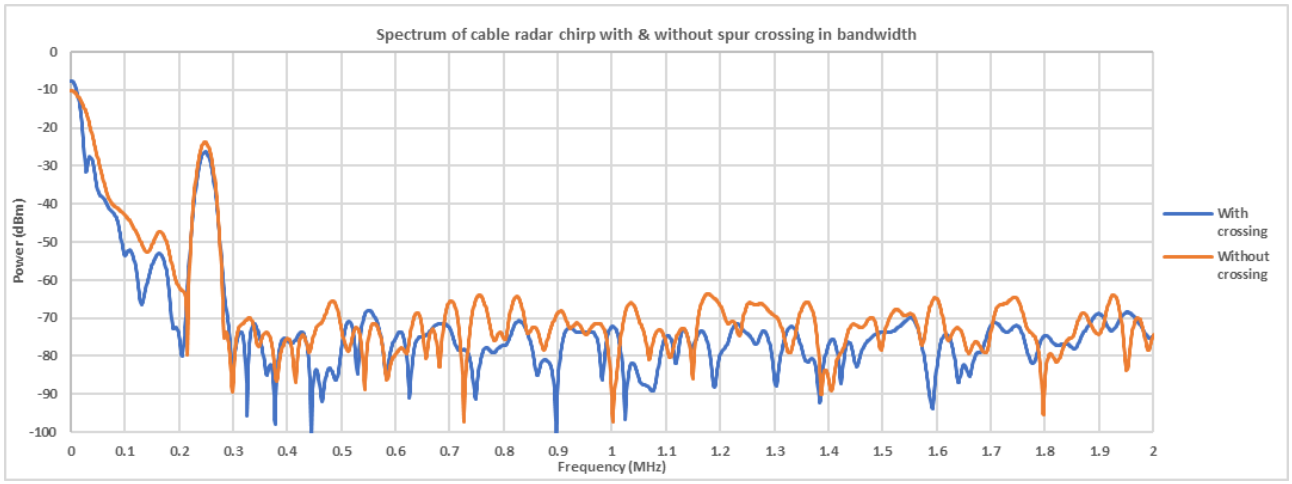

Figure 12: Measured spectra of IF signal with and without spur crossing.

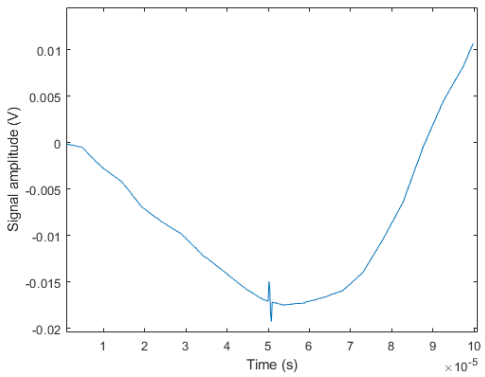

Figure 13: Simulated time domain for -35 dBm spur crossing.

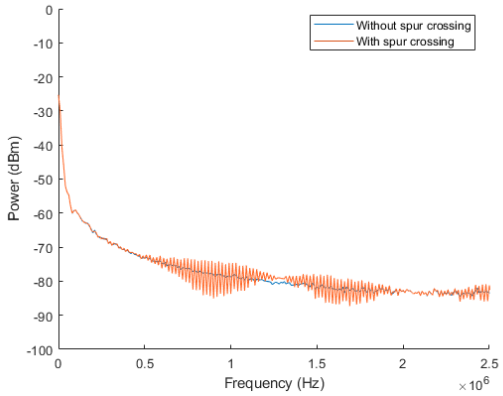

Figure 14: Simulated spectrum for -35 dBm spur crossing.

4. RADAR PHYSICAL DESIGN

The physical design of the radar included several design decisions to reflect the requirements. The primary use of the radar is to validate the point-cloud-based simulation. This will involve measuring propeller micro-Doppler in an indoor setup, where the UAV propeller is located a ~1 m range from the radar. The radar will be operated mono-statically and will be required to view the propeller from multiple aspect (elevation) angles below the plane of rotation of the propeller. However, future experiments with this radar will be conducted outdoors and include bi-static measurements. To accommodate for this, the transmit and receive components are located on separate metal plates which can be attached for mono-static setups and spatially separated when operating bi-statically. This has the added benefit of increasing the mobility of the radar and enables adjusting the aspect angle of the radar when measuring propeller micro-Doppler as will be required for accurate simulation validation. A top-down view of the radar CAD is shown in Figure 15.

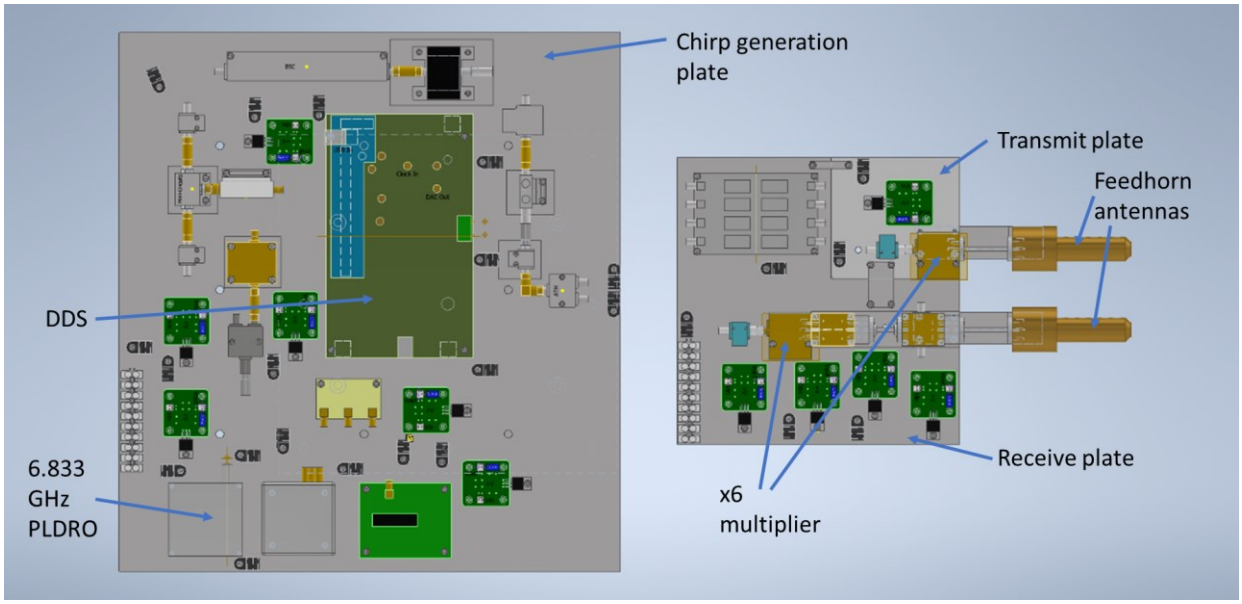

Figure 15: Radar CAD showing the radar in mono-static setup.

As shown, the radar is made up three separate metal plates. The chirp generation plate shown on the left creates, upconverts and amplifies the chirp such that two copies of the output signal are produced from the splitter (on the right-hand-side of the plate) at 15.6 GHz. These two copies of the signal are fed to separate transmit and receive plates, which both multiply this signal to the required 94 GHz. With reference to Figure 1, the plate locations of each radar component can be seen. Shown on the right-hand-side of Figure 15, for the indoor measurements smooth-walled feedhorn antennas fabricated

previously at the University of St Andrews will be used. The physical radar design is such that alternative antennas can be utilized for outdoor measurements including when operating bi-statically.

5. ANTICIPATED RADAR PERFORMANCE

Figure 16 shows the antenna pattern of the smooth-walled feedhorn antennas to be used for indoor simulation validation. These antennas have been chosen because of their large 3 dB beamwidth of 20 degrees and low sidelobes of <-35 dB. A 25 cm propeller will be fully contained within the beamwidth when 71 cm away, which is sufficient for the indoor trials where the propellers will be ~1 m from the radar. These antennas have a directivity of 19.6 dBi and an antenna efficiency in excess of 99%, resulting in a gain of 19.6 dB. The radar parameters are summarized in Table 3.

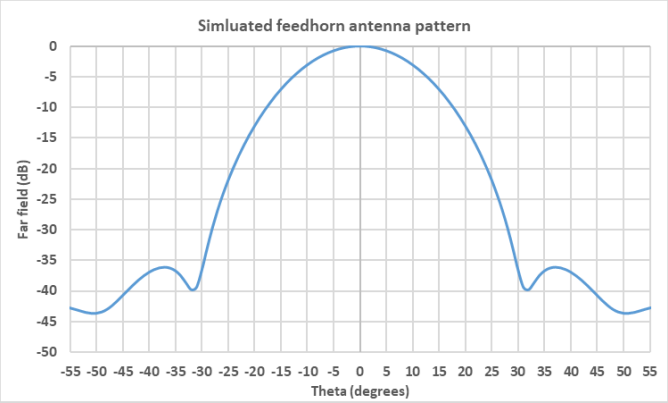

Figure 16: Simulated antenna pattern for smooth-walled feedhorns.

Parameter	***Value***
Antenna 3 dB beamwidth	20 degrees
Antenna gain	19.6 dB
Propeller range	1 m
Propeller RCS	-40 dBsm
Transmitted power	12 dBm

Table 3: Radar parameters.

The estimated receiver noise figure is 8 dB and the total receiver gain is 43 dB, based on data sheet values for the W-band components and lab measurements of the IF chain. Assuming an FFT bin width of 11.2 kHz (resulting from an 89.6 μs chirp length, as per Table 1) the expected receiver noise floor is -80 dBm per bin. For a transmitted power of 12 dBm and an anticipated RCS for the plastic propellers of -40 dBsm, the expected return power after the receiver is -28 dBm. This results in a 51 dB signal-noise-ratio, which is substantial even for small plastic propellers which indicates the radar's suitability for indoor propeller micro-Doppler measurements and ultimately simulation validation. These expected radar performance parameters are given in Table 4.

Parameter	***Value***
Noise figure	8 dB
Total receiver gain	43 dB
Noise floor	-80 dBm
SNR for -40 dBsm propeller for 1 m range	51 dB

Table 4: Expected radar parameters.

The noise figure of the radar receive chain has been measured by performing a Y-factor measurement. A signal at ~7.8 GHz from an Anritsu MG3692C was fed into the multiplier chain and used to pump the LO for the IQ mixer, and the RF port for this mixer was connected to a horn antenna. The IF signal was passed through two Wenteq ABL0050-01-3310 amplifiers, which have a very flat frequency response to > 500 MHz. After these amplifiers, a low pass and high pass filter were used in combination to create an effective bandpass filter (25-250 MHz). The horn antenna was pointed at RF absorber at two different temperatures: one at room temperature (290 K) and another immersed in liquid nitrogen (77 K). A power meter was used to measure the integrated noise power within the IF passband when viewing both temperature absorbers. The difference in noise powers between these two measurements was used to find the noise figure of the radar receive chain. It should be noted that the Wenteq amplifiers were used instead of the BBM in this measurement, because the BBM's maximum frequency of 15 MHz is below the measurement range of the power sensor used. The Wenteq devices have a lower noise figure (~1 dB) than the BBM (~6.2 dB) and, as such, the noise figure of the receive chain using the BBM will be ~1 dB higher than measured here. The measurement was performed over the range of LO frequencies of interest for current and future uses for this radar, as shown in Figure 17. The noise figure varies across the bandwidth of

the radar, largely due to the frequency response of the pre-amplified IQ mixer. However, these measured noise figure values are consistent with the estimated value from Table 4, but may be slightly higher in practice when using the BBM.

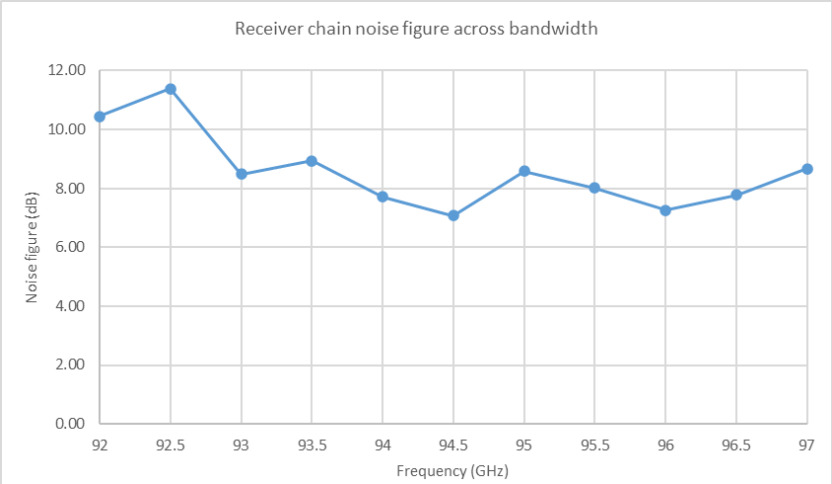

Figure 17: Receiver chain noise figure across bandwidth.

6. FUTURE WORK

A full calibration of the radar with targets of known RCS is required. Following this, the point-cloud-based simulation will need to be validated using this radar. This will involve measuring the propeller micro-Doppler for an indoor lab-based setup at various aspect angles. A photodetector will be used as an independent measure of propeller rotation rate for validation of the Doppler information from the radar. A robust and complete validation of the simulation will be undertaken where simulated scenarios will be recreated as closely as possible and the micro-Doppler information from the simulation compared with the experimental result, obtained using this radar. This validation will be published in due course.

7. CONCLUSION

Micro-Doppler information can be used for differentiating between UAVs and non-UAVs, however, differentiating between UAV models and types is a more complicated problem. A robust study of the micro-Doppler signatures of different UAV components is required along with large amounts of data needed to train future classifiers. To aid with both of these challenges, a point-cloud-based simulation has been developed previously, which generates detailed micro-Doppler spectrograms. This will allow for the study of micro-Doppler signatures with much greater ease than if restricted to experimental data. Furthermore, the simulation can generate large amounts of synthetic data to be used to train classifiers, possibly in conjunction with experimental data. This simulation needs experimental validation, and a radar has been designed for this purpose. This validation will take place indoors to allow for robust recreation of simulated scenarios, but the radar will also be required for future outdoor experiments. Therefore, versatility is essential in the design. The radar has been designed to use both CW and FMCW modes, operate both indoors and outdoors, be mobile, be used mono-statically or bi-statically, and function with a host of antenna types.

In this paper, the requirements and parameters for the validation radar have been explained. The design for the radar has been described in detail, along with the block diagram with relevant design decisions justified. The chirp spectra (when operating in FMCW mode) at key points in the radar chain have been given, including the transmitted chirp spectrum. The radar uses a DDS-based architecture, and an investigation into the prevalence and effect of the spurious signals has been undertaken. Although this analysis did find artifacts corresponding to spur signal crossings in the time-domain, the spectral energy imparted by these events was too small to impact the spectrum significantly. A simulation found that the spur signal crossing artifacts need to be as high as -15 dBc before they affect the spectrum noticeably. The physical radar design has been presented along with a brief explanation of some of the design decisions. The anticipated performance of the radar, including the expected receiver noise figure and signal-to-noise ratio for the indoor propeller micro-Doppler measurements, is given. A Y-factor measurement has been made to confirm the noise figure of the receiver at various frequencies spanning the bandwidth of the radar. Finally, the future work and plans for this radar have been explained.

ACKNOWLEDGEMENTS

The authors acknowledge the financial support of the Engineering and Physical Sciences Council and QinetiQ who are funding MM's PhD.

REFERENCES

[1] "Conflict groups arm consumer drones for terror attacks | E&T Magazine.", 9 April 2021, <https://eandt.theiet.org/content/articles/2021/04/conflict-groups-arm-consumer-drones-to-deliver-death-and-terror/> (11 May 2021).

[2] "Drone stalker jailed for spying on ex-girlfriend - BBC News.", 20 Novemb. 2020, <https://www.bbc.co.uk/news/uk-wales-55018682> (15 April 2021).

[3] "Gatwick-bound plane forced to avoid 'high risk' drone - BBC News.", 28 August 2019, <https://www.bbc.co.uk/news/uk-england-sussex-49494817> (15 April 2021).

[4] Harmanny, R. I. A., De Wit, J. J. M. and Premel-Cabic, G., "Radar micro-Doppler mini-UAV classification using spectrograms and cepstrograms," Int. J. Microw. Wirel. Technol. **7**(3–4), 469–477 (2015).

[5] Rahman, S. and Robertson, D. A., "Multiple drone classification using millimeter-wave CW radar micro-Doppler data," Radar Sens. Technol. XXIV **11408**, 653–661 (2020).

[6] Moore, M., Robertson, D. A. and Rahman, S., "Simulating UAV micro-Doppler using dynamic point clouds," 2022 IEEE Int. Radar Conf. RADAR 2022, accepted for publication.

[7] Rahman, S. and Robertson, D. A., "Radar micro-Doppler signatures of drones and birds at K-band and W-band," Sci. Rep. **8**(1), 1–11 (2018).

[8] Fuhrmann, L., Biallawons, O., Klare, J., Panhuber, R., Klenke, R. and Ender, J., "Micro-Doppler analysis and classification of UAVs at Ka band," Proc. Int. Radar Symp. IRS 2017 (2017).

[9] Bjorklund, S. and Wadstromer, N., "Target Detection and Classification of Small Drones by Deep Learning on Radar Micro-Doppler," 2019 Int. Radar Conf. RADAR 2019 (2019).

[10] Rahman, S. and Robertson, D. A., "Millimeter-wave radar micro-Doppler feature extraction of consumer drones and birds for target discrimination," Proc. SPIE 11003, Radar Sens. Technol. XXIII,(May 2019), 28 (2019).

[11] Drozdowicz, J., Wielgo, M., Samczynski, P., Kulpa, K., Krzonkalla, J., Mordzonek, M., Bryl, M. and Jakielaszek, Z., "35 GHz FMCW drone detection system," Proc. Int. Radar Symp. IRS 2016 **2016-June** (2016).

[12] Rahman, S. and Robertson, D. A., "Classification of drones and birds using convolutional neural networks applied to radar micro-Doppler spectrogram images," IET Radar, Sonar Navig. **15**(6), 653–661 (2019).

[13] Gupta, S., Rai, P. K., Kumar, A., Yalavarthy, P. K. and Cenkeramaddi, L. R., "Target Classification by mmWave FMCW Radars Using Machine Learning on Range-Angle Images," IEEE Sens. J. **21**(18), 19993–20001 (2021).

[14] Oh, B. S., Guo, X. and Lin, Z., "A UAV classification system based on FMCW radar micro-Doppler signature analysis," Expert Syst. Appl. **132**(October), 239–255 (2019).

[15] Rahman, S. and Robertson, D. A., "FAROS-E: A compact and low-cost millimeter wave surveillance radar for real time drone detection and classification," Proc. Int. Radar Symp. IRS 2021 **2021-June**, 978–981 (2021).

[16] Rohde and Schwarz., "FSP Spectrum Analyzer," Oper. Man.(May) (2008).

[17] Gannon, Z. and Tahmoush, D., "Measuring UAV propeller length using micro-doppler signatures," 2020 IEEE Int. Radar Conf. RADAR 2020, 1019–1022, Institute of Electrical and Electronics Engineers Inc. (2020).

[18] Analog devices., "A Technical Tutorial on Digital Signal Synthesis, 1999 | Education | Analog Devices," <https://www.analog.com/en/education/education-library/technical-tutorial-dds.html> (3 March 2022).